Applied Surface Science 531 (2020) 147101

Contents lists available at ScienceDirect

Applied Surface Science

journal homepage: www.elsevier.com/locate/apsusc

In-situ preparation of Ti_3C_2/Ti^{3+}-TiO_2 composites with mosaic structures for the adsorption and Photo-degradation of flowing acetaldehyde under visible light

Xiao Wang[a], Yina Yang[a,b], Guanhong Lu[a], Gansheng Shi[a], Yan Wang[a], Ranran Wang[a], Xiaofeng Xie[a], Jing Sun[a,*]

[a] State Key Laboratory of High Performance Ceramics and Superfine Microstructure, Shanghai Institute of Ceramics, Chinese Academy of Sciences, China
[b] University of Chinese Academy of Sciences, China

ARTICLE INFO

Keywords:
Mosaic structure
Photocatalytic oxidation
Acetaldehyde
Yisible light
Heterojunction composite

ABSTRACT

Photocatalytic degradation has been proven to be an effective way in the elimination of gaseous acetaldehyde. This work provided a facile in-situ method for the fabrication of Ti_3C_2/Ti^{3+}-TiO_2 photocatalysts by oxidizing Ti_3C_2 with H_2O_2. A novel mosaic structure formed by small Ti^{3+}-TiO_2 nanoparticles embedded in Ti_3C_2 layers was obtained by adjusting the synthesis parameters. Compared with pure Ti_3C_2, a 60-fold increase in the BET-SSA was observed in Ti_3C_2/Ti^{3+}-TiO_2 composites, which benefits the capture of the flowing acetaldehyde gas. Self-doped TiO_2 nanoparticles induced by the incomplete oxidation process enabled the photodegradation of acetaldehyde under visible light. Besides, the closely contact between the two components helps the transfer of photon-induced charge carriers from TiO_2 to Ti_3C_2, which suppressed the recombination of electron-hole pairs and promoted the generation of active radicals. Compared with commercial P25, which has almost no catalytic activity under the irradiation of visible light, a degradation efficiency of around 27% was achieved by applying Ti_3C_2/Ti^{3+}-TiO_2 as the photocatalyst. This work provided a new facile method for the in-situ fabrication of heterogeneous structures for the photocatalytic elimination of acetaldehyde under visible light.

1. Introduction

The emission of indoor air pollutants has become a serious public health issue. As one of the common indoor pollutants, acetaldehyde, which may be emitted by glues, paints, decorates etc., is an irritant of the skin, eyes, throat and respiratory tract [1]. Photocatalytic oxidation (PCO) has been proven to be a powerful means in the degradation of indoor acetaldehyde for its low energy consumption [2–5]. In the past decades, TiO_2 has been applied as a promising and environmental-friendly photocatalytic material for the purification of water pollutants due to its strong oxidizing power and easy accessibility [6–9]. However, some intrinsic properties of TiO_2 severely limit its application in the industry of air-purification. On one hand, due to its wide bandgap of 3.2 eV, TiO_2 could only utilize sunlight in the UV region ($\lambda < 388$ nm) [8], which only accounts for 4–5 percent of the total solar energy [10]. On the other hand, unlike aqueous photocatalytic reactions, the low concentration of gaseous pollutants and the short residence time call for photocatalysts with high specific surface area (SSA) and strong affinity for target molecules [10]. The specific surface area of P25, which is about 47 m^2/g, is not high enough for the effective capture of gaseous pollutants [11].

Great efforts have been made to overcome these issues in the past decades. Doping TiO_2 with metal or nonmetal elements was proven to be an effective way in broadening its adsorption spectra [4,12]. By inducing doping levels inside the forbidden band of TiO_2, the utilization of visible light becomes possible for the doping states could act as acceptors or donors of photon-generated electrons. In the recent years, self-doped TiO_2 has been developed as a powerful tool in the photocatalytic degradation of organic molecules [13–16]. In the 1950s, Cronzmeyer and Gilleo [17] found that by reducing rutile TiO_2 in a hydrogen atmosphere, a tail in the visible range appeared in the adsorption spectra of the as-prepared blue crystal. Different synthesis methods for preparing Ti^{3+}-doped TiO_2 has been developed, including calcination under hydrogen atmosphere [18] or with $NaBH_4$ [13,19], metal reduction [14], plasma treatment [20] or partial oxidation of precursors with Ti, Ti(II) and Ti(III). Chen et al. [21] aged TiO_2 in a

* Corresponding author at: State Key Laboratory of High Performance Ceramics and Superfine, Microstructure, Shanghai Institute of Ceramics, Chinese Academy of Sciences, 585 Heshuo Road, Shanghai 201899, China.
E-mail address: jingsun@mail.sic.ac.cn (J. Sun).

https://doi.org/10.1016/j.apsusc.2020.147101
Received 27 March 2020; Received in revised form 24 June 2020; Accepted 26 June 2020
Available online 09 July 2020
0169-4332/

20.0-bar H_2 at 200 °C for 5 days to prepare black TiO_2, which has drawn lots of attention in the photocatalytic degradation of organic pollutants and water splitting. However, most of the preparation methods reported rely on the application of high temperature, dangerous hydrogen gas or long reaction time, which limit the large-scale fabrication and application of self-doped TiO_2. In addition, most of the self-doped TiO_2 fabricated on the basis of P25 or anatase TiO_2 inherited its small specific surface area [22,23], which made it not suitable for the capture and degradation of organic gaseous contaminants. Various conductive 2-D materials such as grapheme [24], g-C_3N_4 [25] and TaS_2 [3] have been widely applied as co-catalysts to promote the separation of charge carriers and increase the total SSA of the photocatalysts. However, most of the composites were synthesized through hydrothermal or electrostatic attraction methods, the agglomeration of TiO_2 particles and the poor interaction between TiO_2 and co-catalysts severely held back the transfer of charge carriers between the two components. MXene is an emerging 2-dimensional material synthesized firstly by Yury Gogotsi's group in 2011 [26]. Much attention has been payed to some typical MXene materials such as Ti_3C_2, Ti_3N_2 and their composites with TiO_2 in the elimination of gaseous pollutants due to their large specific surface area, high conductivity and abundant surface functional groups [27]. As the most investigated MXene material by far, Ti_3C_2 is commonly synthesized through etching the Al layer of Ti_3AlC_2 by HF. Lotfi et al. found that by oxidizing Ti_3C_2 in dry air, Ti atoms would migrate to the surface of the material and bond with O_2, while the left C atoms would bond with each other to form a carbon substrate [28]. Carbon-TiO_2 hybrid materials can be synthesized by controlling the reaction temperature and time. Naguib et al. oxidized Ti_3C_2 in air at 1150 °C for 30 s to get carbon sheets covered by TiO_2 with a specific surface area of ~50 m^2/g [23]. Liu et al. fabricated TiO_2@C/g-C_3N_4 hybrid materials on the basis of Ti_3C_2 and melamine through a facile calcination method [29]. The as-prepared TiO_2@C/g-C_3N_4 exhibited a specific surface area of 49.5 m^2/g. In addition to being calcinated in air or CO_2, hydrothermal treatment was also applied in the oxidation of Ti_3C_2 to fabricate TiO_2/Ti_3C_2 hybrid materials. Gao's results illustrated an improved photocatalytic activity of TiO_2/Ti_3C_2 in the degradation of methyl orange compared with pure TiO_2 or Ti_3C_2 [30]. Peng et al. further controlled the facets of TiO_2 in the hydrothermal reaction with the assistance of the directing reagent $NaBF_4$ [31]. (001) TiO_2/Ti_3C_2 displayed a longer electron lifetime due to the effective separation of photon-generated electron-hole pairs on the interface between TiO_2 and Ti_3C_2, which enabled a significant improved photodegradation of methyl orange. These results indicate that the construction of TiO_2/Ti_3C_2 heterojunctions is an effective way in prolonging the lifetime of electron-hole pairs and promoting the formation of reactive radicals. However, in most cases, Ti atoms are oxidized into Ti^{4+} atoms in TiO_2 due to the difficulties in controlling the oxidation extent in the calcination or hydrothermal methods, no catalytic ability under the irradiation of visible light has been reported to our knowledge. As the oxidation processes in both the calcination treatments and the hydrothermal reactions mainly happen on the surface of Ti_3C_2, only Ti atoms from the outer surface of the Ti_3C_2 could react with the oxidants to form TiO_2 nanoparticles, which is not favorable for the fully contact between the two components. Besides, most of the TiO_2/Ti_3C_2 hetero-structures fabricated previously shows small specific surface areas of around 50 m^2/g, which hinders their application in the field of air purification.

Herein, a facile chemical oxidation method for the fabrication of Ti_3C_2/Ti^{3+}-TiO_2 composites at room temperature was proposed by using H_2O_2 as the oxidant. Through adjusting the reaction parameters, Ti_3C_2/Ti^{3+}-TiO_2 composites with a mosaic structure were synthesized, in which self-doped TiO_2 nanoparticles were embedded in Ti_3C_2 layers. Remarkable specific surface area (~125 m^2/g) and improved adsorption for flowing acetaldehyde molecules were achieved. As expected, the Ti_3C_2/Ti^{3+}-TiO_2 composites exhibited a strong absorption of visible light due to the formation of impurity levels inside the forbidden band of TiO_2. A degradation efficiency of 27% was achieved by applying Ti_3C_2/Ti^{3+}-TiO_2 composite in the photocatalytic degradation of flowing acetaldehyde under the illumination of visible light. Essentially, the remarkable results found in this paper provide a new way for the designing and synthesizing of heterojunction photocatalysts based on TiO_2.

2. Material and methods

2.1. Materials

Ti_3AlC_2 powders (200 meshes) were purchased from Forsman Scientific Corporation (China). 40% hydrofluoric acid (HF, 40%) and 30% hydrogen peroxide (H_2O_2, 30%) were provided by China National Medicines Corporation. Deionized water (18.2 MU cm; Milli-Q Advantage A10, Burlington, USA)) was used as solvents for the synthesis of Ti_3C_2/Ti^{3+}-TiO_2 composites. Acetaldehyde standard gas (1000 ppm) was supplied by Shanghai Weichuang Standard Gas Analytical Technology Co. LTD.

2.2. Synthesis of Ti_3C_2 and Ti_3C_2/Ti^{3+}-TiO_2 composites

Ti_3C_2 powders was synthesized by etching Ti_3AlC_2 powders with HF for 18 h at room temperature according to the method reported by Yang et al. [32]. The Ti_3C_2/Ti^{3+}-TiO_2 composites was obtained by oxidizing Ti_3C_2 with H_2O_2. To be specifically, 0.3 g Ti_3C_2 was dispersed in 10 ml deionized water. 2 ml 30% H_2O_2 was added to the dispersion as an oxidant. The mixed solution was stirred at 40 °C for 10 min to get a black gel. After being dried at the temperature of 60 °C, the gel would turn into the grey Ti_3C_2/Ti^{3+}-TiO_2-1 composite powders.

In a typical synthesis procedure, 0.1 g Ti_3C_2/Ti^{3+}-TiO_2-1 was dispersed in 6 ml deionized water. 30% H_2O_2 with a certain volume ranging from 50 μl to 150 μl was added to the dispersion under agitation. After stirring at room temperature for 10 min, the dispersion was dried at 60 °C to get composite powders with the color gradually changing from green to yellow. The composites synthesized by adding 50 μl and 100 μl H_2O_2 was chosen to study the oxidation process and characterize the performance of Ti_3C_2/Ti^{3+}-TiO_2 composites in the photocatalytic degradation of gaseous acetaldehyde, which were denoted as Ti_3C_2/Ti^{3+}-TiO_2-2 and Ti_3C_2/Ti^{3+}-TiO_2-3, respectively.

2.3. Material characterization

Transmission electron microscopy (TEM) images were obtained on JEM-2100F transmission electron microscope and scanning electron microscopy (SEM) images were acquired on a SU9000 scanning electron microscopy. The thermogravimetric (TG) analysis was carried out on a NETZSCH STA449C thermo analyzer. The UV–vis adsorption spectra were collected by a Perkin Elmer Lambda 950 UV–vis spectrometer. X-ray diffraction (XRD) were characterized by a Rigaku D/max 2550 V XRD system with a monochromatic Cu Kα radiation. X-ray photoelectron spectroscopy (XPS) was measured by a Thermo Fisher Scientific ESCAlab250. XPS samples were prepared by pressing the powders onto the surface of a conductive In particle. An argon sputter ion gun was applied to mitigate surface charging during the XPS tests. All binding energy were calibrated by using contaminated carbon (C1s = 286.4 eV) as a reference. The specific surface area of the samples were tested by a Quadrasorb SI specific surface analyzer. The electron spin resonance (ESR) signals of active radicals was tested on a spectrometer (JES-FA200, JEOL, Japan) by using DMPO as the trapping agent. The electron spin resonance (ESR) signals of Ti^{3+} were tested through the same spectrometer. The photoluminescence spectra (PL) of the samples were obtained with a FLS920 steady-state transient fluorescence spectrometer provided by Edinburgh Instruments with an excitation wavelength of 320 nm.

2.4. Adsorption and photodegradation efficiency of acetaldehyde

0.1 g Ti_3C_2/Ti^{3+}-TiO_2 composites were coated on a 15 cm*7 cm glass slide and placed in a sealed reaction chamber with transparent quartz cover. A mixed gas of acetaldehyde (with an initial concentration of 500 ppm) and air was injected into the chamber continuously with a fixed flow rate of 20 sccm. The concentration of acetaldehyde was analyzed by a gas chromatography connected to the reaction chamber. An adsorption–desorption equilibrium was achieved before starting the light irradiation to characterize the performance of the photocatalysts in capturing acetaldehyde molecules and excluding the effect of adsorption when evaluating the photodegradation ability of the composites. The volume of acetaldehyde was calculated according to Eq. (1):

$$V_{acetaldehyde}\,(\mathrm{ml/g}) = \frac{[\int_0^{90}[A'(t)-A(t)]dt]}{C_0} \times 20\mathrm{ml/min} \times 500 \times 10^{-6}/0.1\mathrm{g} \quad (1)$$

$V_{acetaldehyde}$ (ml/g) stands for the volume of acetaldehyde adsorbed by 1 g of the photocatalyst, A′(t) represents the peak area of the GC signal for acetaldehyde with no photocatalyst in the reaction chamber at t minutes and A(t) stands for the peak area obtained when photocatalysts are applied. The adsorption processes last for 90 min until the adsorption–desorption equilibrium are reached. 20 ml/min is the flow rate of the mixed gas and 500 ppm is the volume content of acetaldehyde in the mixed gas. 0.1 g photocatalysts are applied in the adsorption experiments.

A 500 W Xenon light was then utilized in the experiments, which was placed 20 cm above the reaction chamber. A filter was applied when measuring the performance of the catalysts under visible light. The removal ratio η was calculated according to Eq. (2):

$$\eta = (1 - C/C_0) * 100\% \quad (2)$$

where C_0 stands for the initial concentration of acetaldehyde and C stands for the concentration of acetaldehyde in the gas flow after going through the reaction chamber.

3. Results and discussion:

3.1. Synthesis and characterization of few-layer Ti_3C_2 and Ti_3C_2/Ti^{3+}-TiO_2 composites

Ti_3C_2 was synthesized through etching Ti_3AlC_2 with HF at room temperature for 18 h and freeze-dried to get a black powder. The selective etching of Al atoms leads to the formation of few-layer Ti_3C_2 plates with an average size of 4 μm (Fig S1b). Nanoplates with an accordion-like structure as well as single-layered nanosheets are observed in the as-prepared Ti_3C_2 samples (Figs. 1a, b and S1), indicating the successive etching of Al atoms and the formation of delaminated Ti_3C_2. HRTEM (Fig. 1b) gives the lattice structure of Ti_3C_2 with interlayer spaces of 0.25 nm and 0.23 nm, corresponding well with the (0 0 6) and (1 0 3) planes of Ti_3C_2, respectively [33]. Selective area electron diffraction pattern (Fig. S1d) shows a hexagonal symmetry, indicating that the Ti_3C_2 inherited a hexagonal lattice structure from the initial Ti_3AlC_2 phase [26]. The addition of H_2O_2 rapidly turns the suspension of Ti_3C_2 into a gel within 10 min (Fig S2). As reported previously, Ti atoms in TiC would react with H_2O_2 to form water soluble $[Ti(OH)_3O_2]$ complex, leaving the carbon atoms to form amorphous carbon structures [34]. Similar reaction could be expected in $Ti_3C_2{\cdot}H_2O_2$ would attack the Ti–C bonds and form $[Ti(OH)_3O_2]^-$ complex with Ti, leaving the carbon atoms to form a film-like structure (Fig. S3a). The formation of the $[Ti(OH)_3O_2]^-$ complex and the swelling of Ti_3C_2 layers results in the conversion from a uniform dispersion to a black gel. When drying the gel at the temperature of 60 °C, $[Ti(OH)_3O_2]^-$ complex decomposes into TiO_2 and water and lead to the formation of Ti_3C_2/Ti^{3+}-TiO_2 composites. Nanoparticles with diameters around several nanometers starts to appear on the surface of Ti_3C_2 layers. Lattice fringes with an inter-plane spacing of 0.23 nm are depicted in Fig. 1d, corresponding to the (1 0 3) facet of anatase Ti_3C_2. An interlayer space of around 1 nm could be observed in the HRTEM image of Ti_3C_2/Ti^{3+}-TiO_2-1 (Fig. S3b). In addition to the lattice structure of Ti_3C_2, small particles with an interlayer space of 0.33 nm are also observed in the HRTEM image of Ti_3C_2/Ti^{3+}-TiO_2-1, confirming the formation of small TiO_2 nanoparticles on Ti_3C_2 layers.

By further oxidize Ti_3C_2/Ti^{3+}-TiO_2-1 with H_2O_2, powders with the color of green (Ti_3C_2/Ti^{3+}-TiO_2-2) and yellow (Ti_3C_2/Ti^{3+}-TiO_2-3) could be obtained. Some of the large nanoplates observed in the SEM image of Ti_3C_2 break into small fragments with sizes ranging from tens to a hundred nanometers while small nanoparticles with the size of several nanometers can be seen on the fragments (Fig. S4). The change in the micromorphology can be attributed to the destruction of Ti–C bonds in the Ti_3C_2 skeleton and the formation of TiO_2 nanoparticles. More nanoparticles are observed in the HRTEM image of Ti_3C_2/Ti^{3+}-TiO_2-2 and Ti_3C_2/Ti^{3+}-TiO_2-3 with diameters similar to the ones in Ti_3C_2/Ti^{3+}-TiO_2-1, indicating the further oxidation process mainly causes the formation of new particles instead of the growing of nanoparticles formed during the first stage. Unlike Ti_3C_2/Ti^{3+}-TiO_2-1 and Ti_3C_2/Ti^{3+}-TiO_2-2, no obvious lattice structure can be distinguished around the TiO_2 nanoparticles in Ti_3C_2/Ti^{3+}-TiO_2-3 (Fig. 1h), meaning that the particles might be surrounded by amorphous carbon.

In the purpose of understanding the change in the micromorphology of Ti_3C_2/Ti^{3+}-TiO_2 composites during the oxidation process, the crystallite structure of the samples was revealed by XRD. Compared with the XRD pattern of Ti_3AlC_2 reported previously [35], the (0 0 2) peak at 9.6° shifts to 8.67°, meaning the lattice parameter c increases from 18.4 Å to 20.4 Å due to the successive etching of Al layers. None of the peaks in the XRD pattern of Ti_3C_2 is assigned to TiO_2. The peak at 8.67° is broadened in Ti_3C_2/Ti^{3+}-TiO_2-1 and Ti_3C_2/Ti^{3+}-TiO_2-2, which might be caused by the partial destruction of the Ti_3C_2 skeleton by H_2O_2. However, the existence of this peak meaning that the layered structure is still preserved in the oxidizing process, which corresponds well with the micromorphology of the samples. In contrast, the peak at 8.67° disappears for Ti_3C_2/Ti^{3+}-TiO_2-3, indicating the complete sabotage of the Ti_3C_2 skeleton. The specific surface area (SSA) of the samples were characterized by the Brunauer–Emmett–Teller (BET) analysis (Fig. 2b). For fewer-layered Ti_3C_2, a relatively small BET SSA of 1.957 m^2/g is observed with an type III isothermal curve. The relatively low BET-SSA of Ti_3C_2 severely limits the number of active sites for the adsorption and degradation of gaseous molecules and holds back its application in the air purification field. Oxidizing Ti_3C_2 with H_2O_2 causes a drastic increase in the specific surface area with Ti_3C_2/Ti^{3+}-TiO_2-2 demonstrating a BET-SSA of 125.326 m^2/g, nearly 60 times higher than that of Ti_3C_2. Unlike few-layered Ti_3C_2, type II isothermal curves are observed for Ti_3C_2/Ti^{3+}-TiO_2-1 and Ti_3C_2/Ti^{3+}-TiO_2-2 with average pore diameters of 6.1 nm and 5.3 nm, respectively (Fig. S6). The rapid increase in the specific surface area and the formation of mesopores might be attributed to the swelling of Ti_3C_2 layers happened during the oxidation procedure and the formation of TiO_2 nanoparticles. Interestingly, the BET surface area drops to 13.108 m^2/g in Ti_3C_2/Ti^{3+}-TiO_2-3, which might be attributed to the collapse of the layered structure of Ti_3C_2 and the agglomeration of TiO_2 nanoparticles as observed in the XRD and SEM results. The formation of the mosaic structure of TiO_2 nanoparticles embedded the layered substrates is the main reason for the tremendous increase in the S_{BET} of Ti_3C_2/Ti^{3+}-TiO_2 composites compared with Ti_3C_2.

During the oxidation of Ti_3C_2, the incomplete oxidation of Ti atoms in Ti_3C_2 would result in TiO_2 nanoparticles with abundant oxygen vacancies, which could not only work as active sites for the adsorption and activation of O_2, but also create impurity levels inside the forbidden band of TiO_2 [36]. Electron spin resonance (ESR) tests were carried out to characterize the amount of oxygen vacancies in Ti_3C_2 and as-

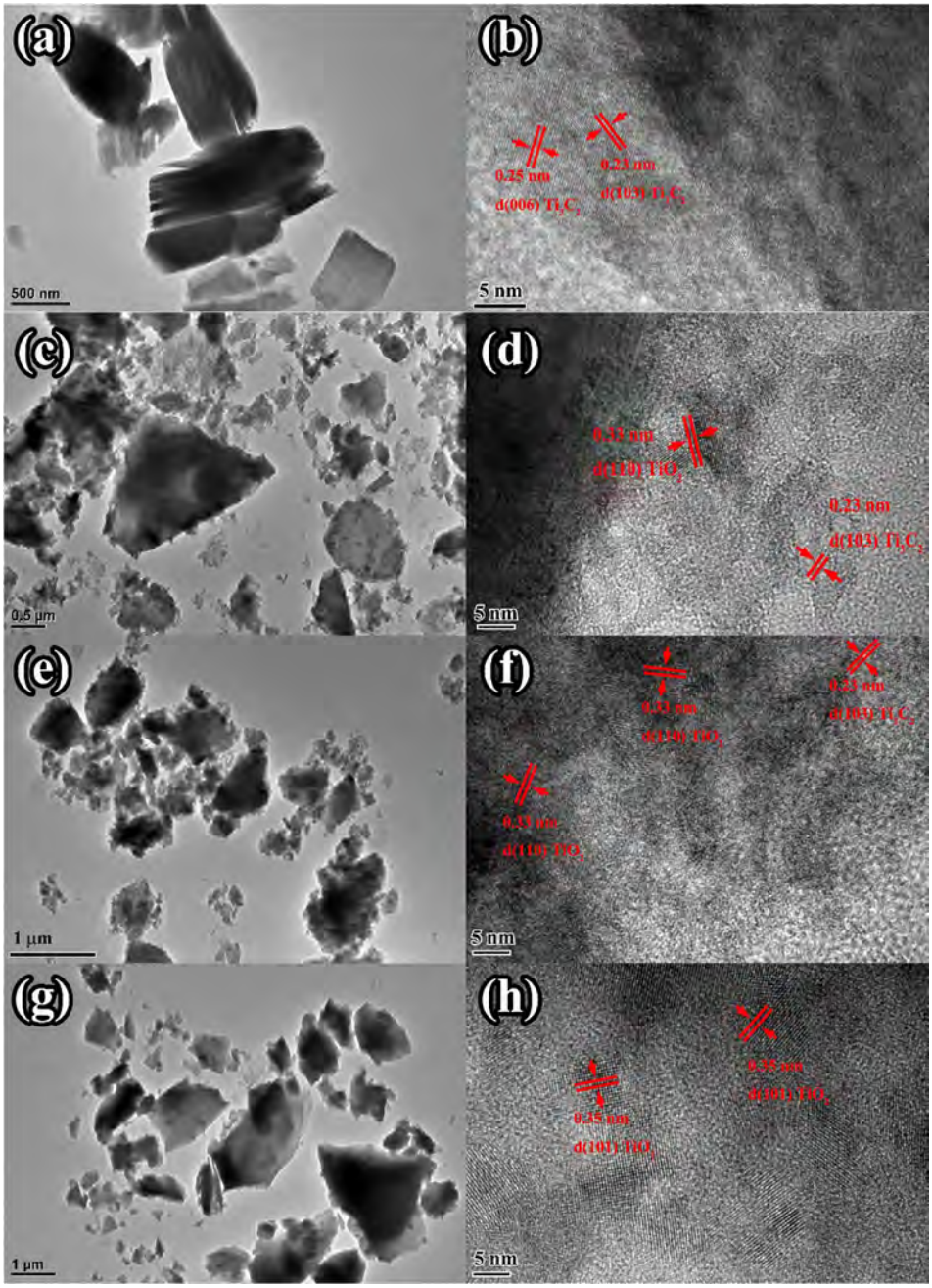

Fig. 1. TEM and HRTEM images of Ti_3C_2 (a, b), Ti_3C_2/Ti^{3+}-TiO_2-1 (c, b), Ti_3C_2/Ti^{3+}-TiO_2-2 (e, f) and Ti_3C_2/Ti^{3+}-TiO_2-3 (g, h).

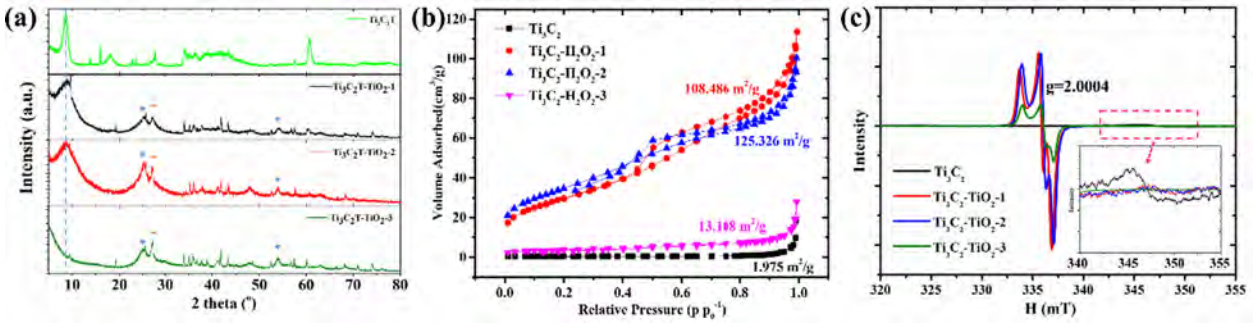

Fig. 2. XRD spectra (a), Nitrogen adsorption-desorption isotherm curves (b) and ESR spectra (c) of Ti_3C_2 and Ti_3C_2/Ti^{3+}-TiO_2 composites.

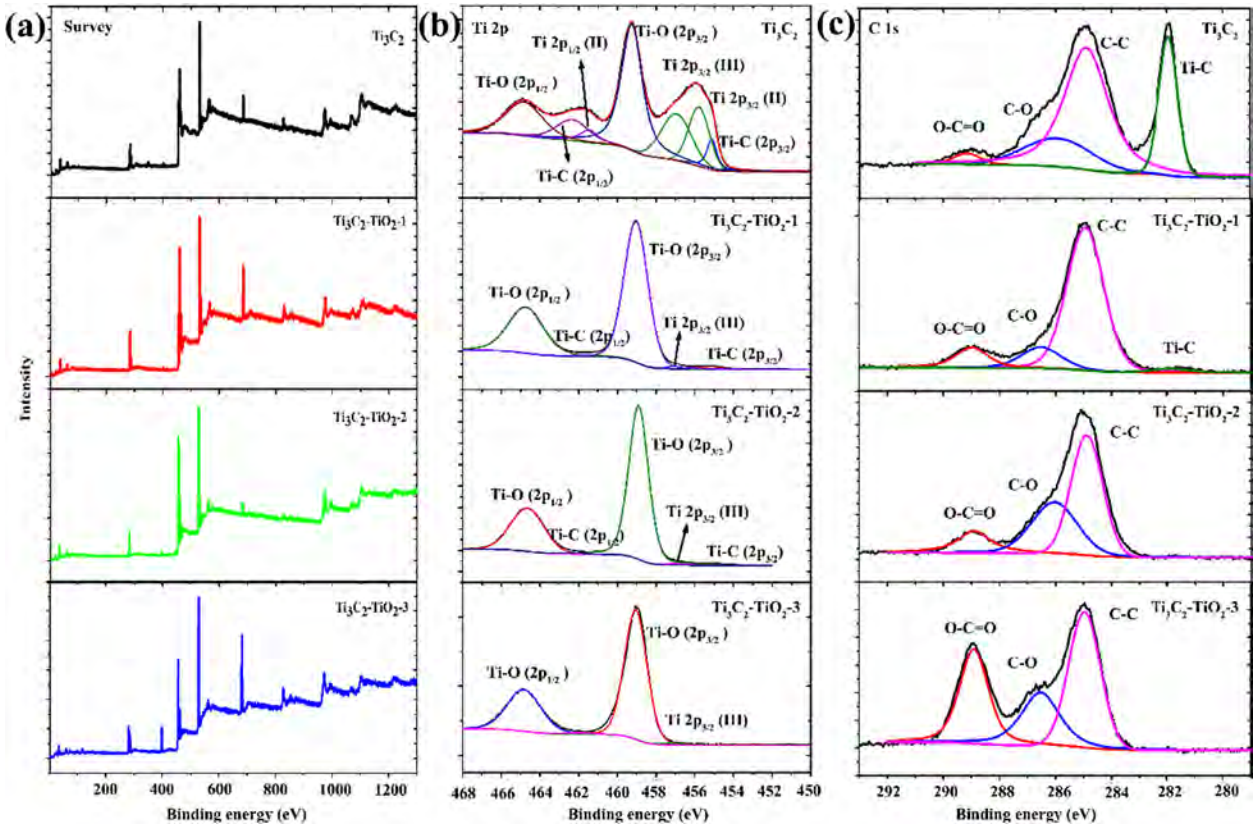

Fig. 3. The XPS survey spectra (a) and the high resolution XPS spectra of Ti 2p (b) and C 1s (c) for Ti_3C_2 and Ti_3C_2/Ti^{3+}-TiO_2 composites.

prepared Ti_3C_2/Ti^{3+}-TiO_2 composites. The signal at the g value of 1.95 is assigned to the Ti^{3+} species in Ti_3C_2 [22]. The formation of Ti_3C_2/Ti^{3+}-TiO_2 composites results in the movement of the Ti^{3+} signal from the g value of 1.95 to 2.004, which might be related to the formation of oxygen vacancies [22]. No obvious signals for oxygen vacancies (g = 2.004) is observed in the ESR spectrum of Ti_3C_2 while Ti_3C_2/Ti^{3+}-TiO_2 composites exhibit a strong signal at g = 2.004, confirming the formation of oxygen-vacancy-rich TiO_2 nanoparticles during the oxidation of Ti_3C_2. Compared with Ti_3C_2/Ti^{3+}-TiO_2-1 and Ti_3C_2/Ti^{3+}-TiO_2-2, a decrease occurred in the intensity of the signals for oxygen vacancies in Ti_3C_2/Ti^{3+}-TiO_2-3, which might be attributed to the further oxidation of unsaturated Ti atoms in TiO_2 nanoparticles by H_2O_2. New signals with g values ranging from 2.01 to 2.03 appears in the ESR spectra of Ti_3C_2/Ti^{3+}-TiO_2-2 and Ti_3C_2/Ti^{3+}-TiO_2-3, which are induced by Ti^{3+} with multiple tetrahedral coordination environments generated during the oxidation of Ti_3C_2 [22]. The in-situ fabrication of Ti_3C_2/Ti^{3+}-TiO_2 composites provides us with a useful way in controlling the formation and amount of oxygen vacancies, which is quite helpful for the optimization of the composite photocatalysts and the effective adsorption and photodegradation of gaseous acetaldehyde.

XPS analysis was also carried out to further understand the oxidation process by characterizing the chemical environment of surface and bulk Ti atoms (Fig. 3b). For as-prepared Ti_3C_2, peaks at 455.0 eV, 457.0 eV, 458.9 eV, 461.3 eV 462.5 eV and 464.6 eV are assigned to Ti–C ($2p_{3/2}$), Ti (III) $2p_{3/2}$, Ti–O ($2p_{3/2}$), Ti(II) $2p_{1/2}$, Ti–C ($2p_{1/2}$) and Ti–O ($2p_{1/2}$) [37,38]. The Ti–O bonds may be originated from the surface functional groups [39]. After the oxidation of Ti_3C_2 by H_2O_2, the intensity of Ti (III), Ti(II) and Ti–C bonds decrease but still can be distinguished in Ti_3C_2/Ti^{3+}-TiO_2-1 and Ti_3C_2/Ti^{3+}-TiO_2-2, which is in accordance with the fact that Ti_3C_2 layers are still preserved in these two samples. On the contrary, peaks for Ti(II) and Ti–C bonds are not observed in the Ti 2p spectra of Ti_3C_2/Ti^{3+}-TiO_2-3, which could be attributed to the damage of Ti–C bonds and the oxidation of Ti(II) during the oxidizing process. The change in the chemical information of Ti atoms could help us in analyzing the formation of Ti_3C_2/Ti^{3+}-TiO_2 composites. According to the XPS spectra, Ti atoms in Ti_3C_2 have combined oxidation states of +2 and +3. H_2O_2 will firstly react with the Ti atoms on the surface of Ti_3C_2. The oxidation of Ti atoms and the break of Ti-C bonds are mainly surface reactions. Fig. 3c gives the C1s spectra of Ti_3C_2 and Ti_3C_2/Ti^{3+}-TiO_2 structures. For as-prepared Ti_3C_2, peaks at 282, 284.9, 286 and 289 eV are assigned to the vibration of C-Ti, C—C, C—O and O—C═O bonds. The peak at 284.9 eV was applied as a reference for the calibration of all binding energy. The C-Ti peaks disappeared in Ti_3C_2/Ti^{3+}-TiO_2 composites while the intensity of C—O and O—C═O bonds increased, which could be attributed to the partially oxidation of C atoms.

3.2. *The performance of Ti_3C_2/Ti^{3+}-TiO_2 composites in the adsorption and PCO of acetaldehyde*

The composites were then applied in the adsorption and degradation of acetaldehyde. Compared with P25 and Ti_3C_2, higher volumes of acetaldehyde are adsorbed when Ti_3C_2/Ti^{3+}-TiO_2 composites are applied as the photocatalysts (Fig. 4a and Table 1). As indicated by Table 1, 0.1 g Ti_3C_2/Ti^{3+}-TiO_2-2 exhibit a strong affinity to acetaldehyde with 0.1004 ml gaseous acetaldehyde being adsorbed on its surface, followed by Ti_3C_2/Ti^{3+}-TiO_2-1 (0.0753 ml) due to the high BET SSA of these two samples. The volume of acetaldehyde absorbed on 0.1 g Ti_3C_2 and Ti_3C_2/Ti^{3+}-TiO_2-3 are 0.0568 ml and 0.0598 ml, respectively, in accordance with their smaller BET SSA. Interestingly, though exhibiting much smaller BET SSA, the volumes of acetaldehyde absorbed on Ti_3C_2 and Ti_3C_2/Ti^{3+}-TiO_2-3 are similar to that of TiO_2, which might be related to the more active adsorption sites provided by the unsaturated Ti atoms in Ti_3C_2 and its composites.

The performance of the composites in the photocatalytic degradation under both visible light (> 420 nm) and Xenon light were then

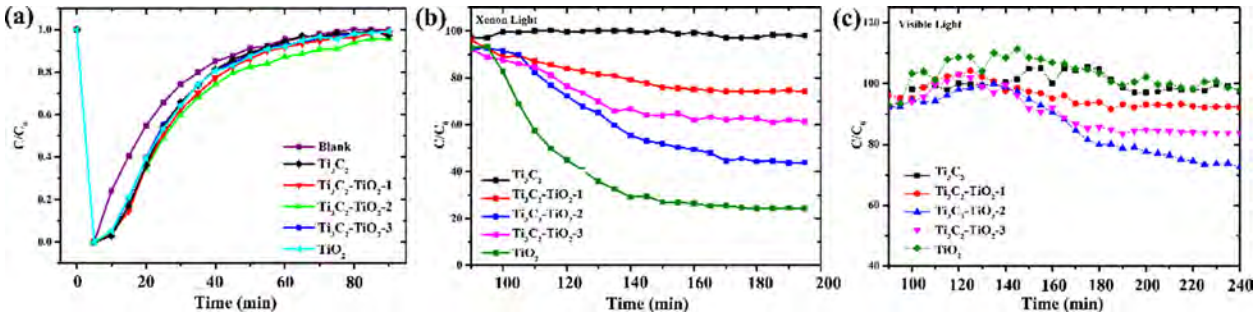

Fig. 4. (a) The dynamic adsorption of acetaldehyde by Ti_3C_2, P25 and Ti_3C_2/Ti^{3+}-TiO_2 composites with no light illumination. The degradation of acetaldehyde by Ti_3C_2, P25 and Ti_3C_2/Ti^{3+}-TiO_2 composites under the illumination of Xenon light (b) and visible light (c).

tested to testify the applicability of the Ti_3C_2/Ti^{3+}-TiO_2 in the photo-elimination of gaseous acetaldehyde. No degradation of acetaldehyde is observed when using pure Ti_3C_2 as the photocatalysts. Among the Ti_3C_2/Ti^{3+}-TiO_2 composites, Ti_3C_2/Ti^{3+}-TiO_2-2 shows the best performance in eliminating gaseous acetaldehyde. A comparison between the performance of Ti_3C_2/Ti^{3+}-TiO_2 composites and commercial P25 is also given in Fig. 4. The performance of Ti_3C_2/Ti^{3+}-TiO_2 composites are not as good as P25 under the irradiation of Xenon light, which might be attributed to the smaller amount of active TiO_2 photocatalysts in Ti_3C_2/Ti^{3+}-TiO_2 compared with P25. However, under the irradiation of visible light (> 420 nm) (Fig. 4c), almost no degradation of acetaldehyde was observed when TiO_2-P25 or pure Ti_3C_2 is applied as the photocatalysts while Ti_3C_2/Ti^{3+}-TiO_2 composites could degrade 27% of the flowing acetaldehyde.

3.3. Mechanism of the enhanced photocatalytic activity of Ti_3C_2/Ti^{3+}-TiO_2 composites

Interestingly, among all Ti_3C_2/Ti^{3+}-TiO_2 composites, Ti_3C_2/Ti^{3+}-TiO_2-2 gives the best performance other than Ti_3C_2/Ti^{3+}-TiO_2-3, which is supposed to have the largest amount of active TiO_2 nanoparticles. This phenomenon might be related to the larger S_{BET} of Ti_3C_2/Ti^{3+}-TiO_2-2 and the heterojunction structure formed by the TiO_2 nanoparticles and the surrounding Ti_3C_2 substrate. As reported previously, Ti_3C_2 terminated by –OH or –F groups could be regarded as a metallic conductor or semiconductor with narrow band-gaps ranging from 0.05 ~ 0.1 eV [26]. Though the application of Ti_3C_2 in the photo-degradation of gaseous pollutants is limited due to its unsuitable valence and conduction band level, it could work as an efficient co-catalyst with TiO_2 by promoting the separation of photon-induced electron-hole pairs.

In addition to the adsorption of target molecules, the utilization of light, the effective separation of photon-induced electron-hole pairs and the generation of reactive radicals are also key factors in determining the performance of photocatalysts. The UV–vis spectra and the PL spectra of the samples are given in Fig. 5. No absorption of visible light is observed for TiO_2 due to its large bandgap while a strong absorbance could be seen in the whole visible and ultraviolet range for Ti_3C_2. As the oxidation extent increases, the absorbance of light with high wavelength gradually decreases. For Ti_3C_2/Ti^{3+}-TiO_2-3, the absorbance spectrum exhibits a similar form as TiO_2 but a much higher absorbance edge at around 550 nm, which could be attribute to the formation of self-doped Ti^{3+}-TiO_2 nanoparticles. The excitation of electrons in Ti_3C_2/Ti^{3+}-TiO_2 composites may happen in the visible range, which is helpful for the effective utilization of the sunlight.

Fig. 5b gives the PL spectra of the samples excited by 320 nm light. As reported previously, the PL intensity is mainly related to the recombination rate of electron-hole pairs [40] and the intrinsic free charge density of the material [41]. Among all the samples, Ti_3C_2 shows a relative weaker PL signal, which is mainly a result of its intrinsic low free charge carrier density compared with TiO_2. The formation of Ti^{3+}-TiO_2 nanoparticles would affect the PL spectra in two ways. On one hand, Ti^{3+}-TiO_2 nanoparticles formed during the oxidation process would increase the free charge density of the Ti_3C_2/Ti^{3+}-TiO_2 composites. On the other hand, the formation of heterojunction structure could enable the injection of photon-induced holes from Ti^{3+}-TiO_2 particles to Ti_3C_2 [33]. As an excellent charge storage host [42], Ti_3C_2 could accept the free charge carriers generated in TiO_2 and facilitate the effective separation of photon-induced electron-hole pairs, which would result in the lower PL intensity. Under the antagonism action of these two factors, Ti_3C_2/Ti^{3+}-TiO_2-1 shows a weaker PL signal compared with Ti_3C_2. The lack of active TiO_2 nanoparticles limits the free charge density of Ti_3C_2/Ti^{3+}-TiO_2-1, which in turn leads to its poor degradation efficiency. Further oxidation process would generate more Ti^{3+}-TiO_2 particles in Ti_3C_2/Ti^{3+}-TiO_2-2 and Ti_3C_2/Ti^{3+}-TiO_2-3, and therefore stronger PL signals of these two samples. As illustrated by the weight ratio calculated according to the TG curves (Table S1), Ti_3C_2/Ti^{3+}-TiO_2-3 has the most amount of TiO_2 nanoparticles, which ensures the generation of the highest density of free carriers. Besides, the collapse of Ti_3C_2 layers is harmful to the spatial separation of electron-hole pairs. Therefore, the strongest PL signal is observed in Ti_3C_2/Ti^{3+}-TiO_2-3. Though exhibiting a strong ability in generating free charge carriers, the rapid recombination and short lifetime of electrons and holes in Ti_3C_2/Ti^{3+}-TiO_2-3 severely limits its performance in the photo-degradation of acetaldehyde. Compared with Ti_3C_2/Ti^{3+}-TiO_2-1 and Ti_3C_2/Ti^{3+}-TiO_2-3, Ti_3C_2/Ti^{3+}-TiO_2-2 not only has a large amount of Ti^{3+}-TiO_2 nanoparticles, but also possesses a mosaic heterojunction structure, which prevents the recombination of electron-hole pairs and extends the lifetime of free charge carriers. These two effects ensures the generation of enough active radicals for the photo-degradation of acetaldehyde.

As reported previously, the adsorbed acetaldehyde molecules are mainly oxidized by the $\cdot O_2^-$ and ·OH radicals [24]. The characterization of reactive radicals would be much helpful for us to predict and understand the performance of these composite photocatalysts in the PCO of acetaldehyde. The ESR spin trapping technique was applied to

Table 1
The BET specific surface area of Ti_3C_2 and Ti_3C_2/Ti^{3+}-TiO_2 composites and the corresponding volume of the acetaldehyde absorbed by the composites.

	TiO_2	Ti_3C_2	Ti_3C_2/Ti^{3+}-TiO_2-1	Ti_3C_2/Ti^{3+}-TiO_2-2	Ti_3C_2/Ti^{3+}-TiO_2-3
BET SSA (m^2/g)	58.403	1.975	108.486	125.326	13.108
$V_{acetaldehyde}$ (ml/g)	0.592	0.568	0.753	1.004	0.598

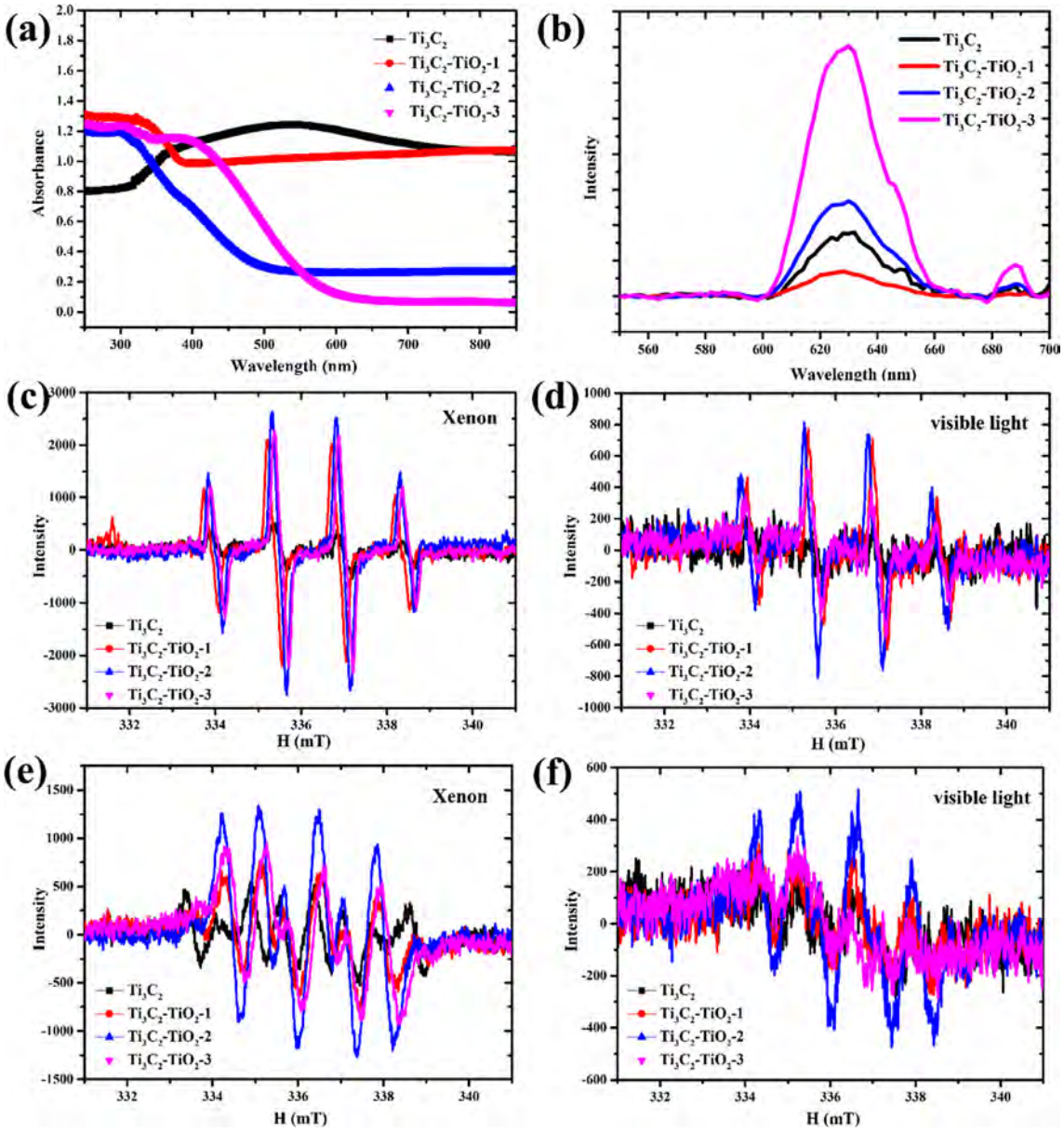

Fig. 5. The UV–vis spectra (a) and the PL spectra of Ti_3C_2 and Ti_3C_2/Ti^{3+}-TiO_2 composites. The DMPO spin-trapping ESR spectra of Ti_3C_2 and Ti_3C_2/Ti^{3+}-TiO_2 composites in aqueous dispersion (c, e) and methanol dispersion (d, f).

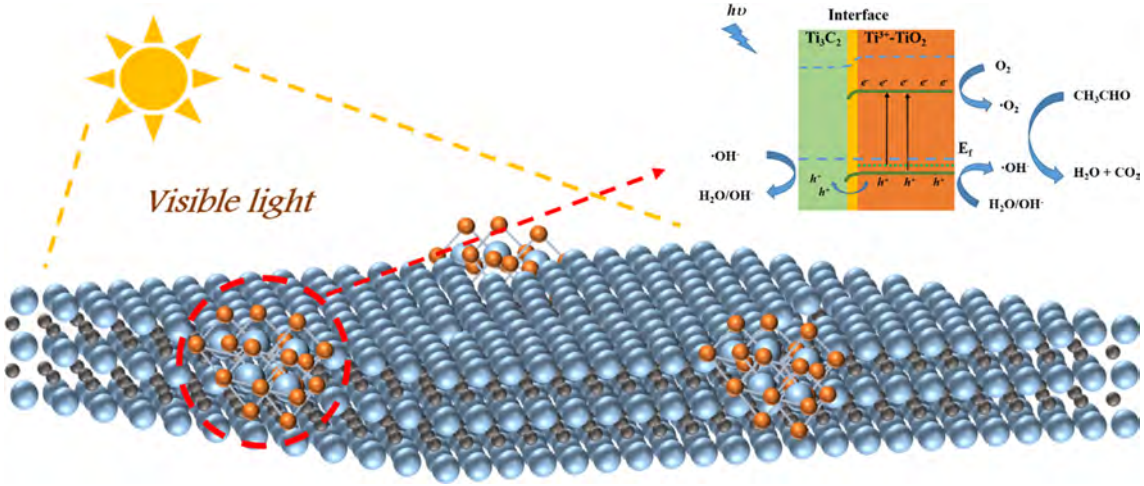

Fig. 6. Scheme of the Ti_3C_2/Ti^{3+}-TiO_2 composites and the transfer of charge carriers under the irradiation of visible light.

evaluate the ability of different photocatalysts in generating reactive radicals. The four-line ESR signals with intensity ratios of 1:2:2:1 (Fig. 5c and d) and 1:1:1:1 (Fig. 5e and f) in the spectra are assigned to the signals of ·OH and $\cdot O_2^-$ radicals, respectively. Both Ti_3C_2 and Ti_3C_2/Ti^{3+}-TiO_2 composites generate $\cdot O_2^-$ and ·OH radicals after being irradiated by xenon light for 5 min (Fig. 5c and e). The intensities of $\cdot O_2^-$ and ·OH radicals generated by Ti_3C_2 are relatively low, which might be caused by the insufficient energy of photon-induced electrons and holes for the generation of the reactive radicals. Among all the Ti_3C_2/Ti^{3+}-TiO_2 composites, Ti_3C_2/Ti^{3+}-TiO_2-2 gives the strongest signal for the two reactive radicals, which makes it the most promising photocatalyst for the PCO of organic pollutants. The generation of more reactive radicals by Ti_3C_2/Ti^{3+}-TiO_2-2 might be a combined result of the larger amount of TiO_2 nanoparticles compared with Ti_3C_2/Ti^{3+}-TiO_2-1, the increased adsorption of O_2 and H_2O due to its large BET surface area and the effective separation of electron-hole pairs. The generation of reactive radicals were also characterized by using a filter to cut off the light with wavelength lower than 420 nm. Compared with the intensity of ·OH and $\cdot O_2^-$ radicals under xenon light, spectra of these two reactive radicals obtained under the irradiation of visible light is slightly lower, while a similar trend between different samples is observed. The generation of reactive radicals is much more efficient in Ti_3C_2/Ti^{3+}-TiO_2-2 than other composites or Ti_3C_2, which is in accordance with the photocatalytic performance of the samples.

Fig. 6 gives the illustration for the structure and the charge transfer in the Ti_3C_2/Ti^{3+}-TiO_2 composites and the proposed mechanism for the photocatalytic reaction. When precisely control the oxidation process, a mosaic structure with Ti^{3+} self-doped TiO_2 nanoparticles embedded in the Ti_3C_2 layers could be synthesized. The existence of unsaturated Ti^{3+} ions would induce defect states inside the forbidden area of TiO_2 and enabled the generation of active electron-hole pairs under the irradiation of visible light. Theoretically calculation has proven that Ti_3C_2 terminated with both −O and −OH groups are metallic conductors [43], which makes them great candidate for accepting charge carriers generated by TiO_2. Due to the formation of Schottky junction at the interface, the electron flow from Ti^{3+}-TiO_2 to Ti_3C_2 is suppressed, while photon-induced holes generated in TiO_2 could be injected into Ti_3C_2 substrates [33]. The spatial separation could effectively prevent the recombination of electron-hole pairs and enable the formation of more reactive radicals. The produced $\cdot O_2^-$ and ·OH radicals would act as a strong oxidizer in converting acetaldehyde into CO_2 and water. The control over the oxidation extent to form an embedded structure with enough self-doped TiO_2 nanoparticles would be an effective way in optimizing the performance of Ti_3C_2/Ti^{3+}-TiO_2 composites.

4. Conclusion

In conclusion, a facile oxidation method was proposed for the synthesis of Ti_3C_2/Ti^{3+}-TiO_2 composites, which could be applied as an efficient photocatalyst for the degradation of gaseous acetaldehyde. Small TiO_2 nanoparticles with an average diameter of around 5 nm would form on Ti_3C_2 substrates, which exhibited a large BET surface area and a strong affinity for acetaldehyde molecules. By adjusting the concentration of the oxidant in the synthesis procedure, the amount of TiO_2 nanoparticles and the structure of the composites could be well controlled. Results indicated that the composite with a structure of TiO_2 nanoparticles embedded in the Ti_3C_2 layers showed the best performance in absorbing and degrading gaseous acetaldehyde. The embedded structure guarantees the closely contact and effective charge transfer between the two components while the formation of enough Ti^{3+}-TiO_2 nanoparticles enables the generation of active electron-hole pairs. Photon-induced charge carriers generated in TiO_2 would transfer to Ti_3C_2 substrate, which facilitates the effective separation of electron-hole pairs in TiO_2 and promotes the formation of reactive radicals. The existence of unsaturated Ti atoms enables the effective utilization of visible light by the Ti_3C_2-TiO_2 composites. 27% of acetaldehyde could be degraded when Ti_3C_2/Ti^{3+}-TiO_2-2 is used as the photocatalyst under visible light, which is much higher compared with commercial TiO_2 photocatalysts. This study provides new sights into the design of photocatalysts for the elimination of indoor air pollutants with low concentration.

Declaration of Competing Interest

The authors declare that they have no known competing financial interests or personal relationships that could have appeared to influence the work reported in this paper.

Acknowledgements

This work was financially supported by the National Key Research and Development Program of China (2016YFA0203000), Shanghai Sailing Program (18YF1426800), the National Natural Science Foundation of China (Grant No. 41907303), the NSFC-DFG bilateral organization program (Grant No. 51761135107) and the Scientific Research Program of Science and Technology Commission of Shanghai Municipality (Grant No. 19DZ1202600).

Appendix A. Supplementary data

Supplementary data to this article can be found online at https://doi.org/10.1016/j.apsusc.2020.147101.

References

[1] E. Uhde, T. Salthammer, Impact of reaction products from building materials and furnishings on indoor air quality—a review of recent advances in indoor chemistry, Atmos. Environ. 41 (2007) 3111–3128.
[2] J. Mo, Y. Zhang, Q. Xu, J.J. Lamson, R. Zhao, Photocatalytic purification of volatile organic compounds in indoor air: a literature review, Atmos. Environ. 43 (2009) 2229–2246.
[3] Q. Zeng, X. Wang, X. Xie, G. Lu, Y. Wang, S. Cheng Lee, J. Sun, TiO_2/TaS_2 with superior charge separation and adsorptive capacity to the photodegradation of gaseous acetaldehyde, Chem. Eng. J. 379 (2020) 122395.
[4] Z. Rao, X. Xie, X. Wang, A. Mahmood, S. Tong, M. Ge, J. Sun, Defect chemistry of Er^{3+}-doped TiO_2 and its photocatalytic activity for the degradation of flowing gas-phase VOCs, J. Phys. Chem. C 123 (2019) 12321–12334.
[5] X. Dai, Y. Wang, X. Wang, S. Tong, X. Xie, Polarity on adsorption and photocatalytic performances of N-GR/TiO_2 towards gaseous acetaldehyde and ethylene, Appl. Surf. Sci. 485 (2019) 255–265.
[6] M.R. Hoffmann, S.T. Martin, W. Choi, D.W. Bahnemann, Environmental applications of semiconductor photocatalysis, Chem. Rev. 95 (1995) 69–96.
[7] K. Hashimoto, H. Irie, A. Fujishima, TiO_2 photocatalysis: a historical overview and future prospects, Jpn. J. Appl. Phys. 44 (2005) 8269–8285.
[8] Z. Shayegan, C.-S. Lee, F. Haghighat, TiO_2 photocatalyst for removal of volatile organic compounds in gas phase – a review, Chem. Eng. J. 334 (2018) 2408–2439.
[9] Q. Guo, C. Zhou, Z. Ma, X. Yang, Fundamentals of TiO_2 photocatalysis: concepts, mechanisms, and challenges, Adv. Mater. (2019) e1901997.
[10] M. Schreck, M. Niederberger, Photocatalytic gas phase reactions, Chem. Mater. 31 (2019) 597–618.
[11] C.-C. Nguyen, D.T. Nguyen, T.-O. Do, A novel route to synthesize C/Pt/TiO_2 phase tunable anatase–Rutile TiO_2 for efficient sunlight-driven photocatalytic applications, Appl. Catal. B 226 (2018) 46–52.
[12] Q. Xiang, J. Yu, W. Wang, M. Jaroniec, Nitrogen self-doped nanosized TiO2 sheets with exposed 001 facets for enhanced visible-light photocatalytic activity, Chem. Commun. 47 (2011) 6906–6908.
[13] Y. Liu, Q. Zhu, X. Li, G. Zhang, Y. Liu, S. Tang, E. Sharman, J. Jiang, Y. Luo, Combining high photocatalytic activity and stability via subsurface defects in TiO_2, J. Phys. Chem. C 122 (2018) 17221–17227.
[14] X. Yan, Y. Li, T. Xia, Black titanium dioxide nanomaterials in photocatalysis, Int. J. Photoenergy 2017 (2017) 1–16.
[15] G. Yin, X. Huang, T. Chen, W. Zhao, Q. Bi, J. Xu, Y.-F. Han, F. Huang, Hydrogenated blue titania for efficient solar-to-chemical conversions: preparation, characterization, and reaction mechanism of CO_2 reduction, ACS Catal. (2017).
[16] X. Pan, M.Q. Yang, X. Fu, N. Zhang, Y.J. Xu, Defective TiO_2 with oxygen vacancies: synthesis, properties and photocatalytic applications, Nanoscale 5 (2013) 3601–3614.
[17] D.C. Cronemeyer, M.A. Gilleo, The optical absorption and photoconductivity of rutile, Phys. Rev. 82 (1951) 975–976.
[18] A. Naldoni, M. Allieta, S. Santangelo, M. Marelli, F. Fabbri, S. Cappelli, C.L. Bianchi, R. Psaro, V. Dal Santo, Effect of nature and location of defects on bandgap narrowing in black TiO_2 nanoparticles, J. Am. Chem. Soc. 134 (2012) 7600–7603.

[19] H. Tan, Z. Zhao, M. Niu, C. Mao, D. Cao, D. Cheng, P. Feng, Z. Sun, A facile and versatile method for preparation of colored TiO_2 with enhanced solar-driven photocatalytic activity, Nanoscale 6 (2014) 10216–10223.
[20] Y. Yan, M. Han, A. Konkin, T. Koppe, D. Wang, T. Andreu, G. Chen, U. Vetter, J.R. Morante, P. Schaaf, Slightly hydrogenated TiO_2 with enhanced photocatalytic performance, J. Mater. Chem. A 2 (2014) 12708–12716.
[21] X. Chen, L. Liu, P.Y. Yu, S.S. Mao, Increasing solar absorption for photocatalysis with black hydrogenated titanium dioxide nanocrystals, Science 331 (2011) 746–750.
[22] Y. Xu, S. Wang, J. Yang, B. Han, R. Nie, J. Wang, J. Wang, H. Jing, In-situ grown nanocrystal TiO_2 on 2D Ti3C2 nanosheets for artificial photosynthesis of chemical fuels, Nano Energy 51 (2018) 442–450.
[23] M. Naguib, O. Mashtalir, M.R. Lukatskaya, B. Dyatkin, C. Zhang, V. Presser, Y. Gogotsi, M.W. Barsoum, One-step synthesis of nanocrystalline transition metal oxides on thin sheets of disordered graphitic carbon by oxidation of MXenes, Chem. Commun. 50 (2014) 7420–7423.
[24] W. Lin, X. Xie, X. Wang, Y. Wang, D. Segets, J. Sun, Efficient adsorption and sustainable degradation of gaseous acetaldehyde and o-xylene using rGO-TiO_2 photocatalyst, Chem. Eng. J. 349 (2018) 708–718.
[25] C. Wang, Y. Zhao, H. Xu, Y. Li, Y. Wei, J. Liu, Z. Zhao, Efficient Z-scheme photocatalysts of ultrathin g-C_3N_4-wrapped Au/TiO_2-nanocrystals for enhanced visible-light-driven conversion of CO2 with H2O, Appl. Catal. B: Environ. (2019) 118314.
[26] M. Naguib, M. Kurtoglu, V. Presser, J. Lu, J. Niu, M. Heon, L. Hultman, Y. Gogotsi, M.W. Barsoum, Two-dimensional nanocrystals produced by exfoliation of Ti_3AlC_2, Adv. Mater. 23 (2011) 4248–4253.
[27] Y. Zhang, L. Wang, N. Zhang, Z. Zhou, Adsorptive environmental applications of MXene nanomaterials: a review, RSC Adv. 8 (2018) 19895–19905.
[28] R. Lotfi, M. Naguib, D.E. Yilmaz, J. Nanda, A.C.T. van Duin, A comparative study on the oxidation of two-dimensional Ti_3C_2 MXene structures in different environments, J. Mater. Chem. A 6 (2018) 12733–12743.
[29] Q. Liu, L. Ai, J. Jiang, MXene-derived TiO_2@C/g-C_3N_4 heterojunctions for highly efficient nitrogen photofixation, J. Mater. Chem. A 6 (2018) 4102–4110.
[30] Y. Gao, L. Wang, A. Zhou, Z. Li, J. Chen, H. Bala, Q. Hu, X. Cao, Hydrothermal synthesis of TiO_2/Ti_3C_2 nanocomposites with enhanced photocatalytic activity, Mater. Lett. 150 (2015) 62–64.
[31] C. Peng, H. Wang, H. Yu, F. Peng, (111) TiO2-x /Ti3C2: synergy of active facets, interfacial charge transfer and Ti3+ doping for enhance photocatalytic activity, Mater. Res. Bull. 89 (2017) 16–25.
[32] Y. Yang, L. Shi, Z. Cao, R. Wang, J. Sun, Strain sensors with a high sensitivity and a wide sensing range based on a $Ti_3C_2T_x$(MXene) nanoparticle-nanosheet hybrid network, Adv. Funct. Mater. 29 (2019) 1807882.
[33] C. Peng, X. Yang, Y. Li, H. Yu, H. Wang, F. Peng, Hybrids of two-dimensional Ti3C2 and TiO2 exposing 001 facets toward enhanced photocatalytic activity, ACS Appl. Mater. Interfaces 8 (2016) 6051–6060.
[34] Y. Ren, W. Hu, Facile synthesis of nanostructured anatase titania with controllable morphology via oxidation of TiC with hydrogen peroxide, J. Nanomater. 2016 (2016) 1–11.
[35] A. Feng, Y. Yu, Y. Wang, F. Jiang, Y. Yu, L. Mi, L. Song, Two-dimensional MXene Ti_3C_2 produced by exfoliation of Ti_3AlC_2, Mater. Des. 114 (2017) 161–166.
[36] Q. Chen, H. Wang, C. Wang, R. Guan, R. Duan, Y. Fang, X. Hu, Activation of molecular oxygen in selectively photocatalytic organic conversion upon defective TiO_2 nanosheets with boosted separation of charge carriers, Appl. Catal. B: Environ. (2019) 118258.
[37] Y. Fang, Z. Liu, J. Han, Z. Jin, Y. Han, F. Wang, Y. Niu, Y. Wu, Y. Xu, High-performance electrocatalytic conversion of N2 to NH3 using oxygen-vacancy-rich TiO_2 in situ grown on $Ti_3C_2T_x$ MXene, Adv. Energy Mater. 9 (2019) 1803406.
[38] Y. Liu, Y. Li, S. Yang, Y. Lin, J. Zuo, H. Liang, F. Peng, Revealing the relationship between photocatalytic properties and structure characteristics of TiO_2 reduced by hydrogen and carbon monoxide treatment, ChemSusChem 11 (2018) 2766–2775.
[39] H. Huang, Y. Song, N. Li, D. Chen, Q. Xu, H. Li, J. He, J. Lu, One-step in-situ preparation of N-doped TiO_2@C derived from Ti_3C_2 MXene for enhanced visible-light driven photodegradation, Appl. Catal. B: Environ. (2019).
[40] G.D. Gilliland, Photoluminescence spectroscopy of crystalline semiconductors, Mater. Sci. Eng.: R: Rep. 18 (1997) 99–399.
[41] Y. Lin, Q. Zhang, Y. Li, Y. Liu, K. Xu, J. Huang, X. Zhou, F. Peng, The evolution from a typical type-I CdS/ZnS to type-II and Z-scheme hybrid structure for efficient and stable hydrogen production under visible light, ACS Sustain. Chem. Eng. 8 (2020) 4537–4546.
[42] M. Okubo, A. Sugahara, S. Kajiyama, A. Yamada, MXene as a charge storage host, Acc. Chem. Res. 51 (2018) 591–599.
[43] M. Khazaei, A. Ranjbar, M. Arai, T. Sasaki, S. Yunoki, Electronic properties and applications of MXenes: a theoretical review, J. Mater. Chem. C 5 (2017) 2488–2503.